Nanoscale

Extracellular Electron Transfer Across Bio-Nano Interfaces for CO2 Electroreduction

Journal:	*Nanoscale*
Manuscript ID	NR-ART-10-2020-007611.R1
Article Type:	Paper
Date Submitted by the Author:	10-Dec-2020
Complete List of Authors:	Li, Zhaodong; National Renewable Energy Laboratory Xiong, Wei; National Renewable Energy Laboratory, Biosciences Center Tremolet de Villers, Bertrand; National Renewable Energy Laboratory (NREL), Chemistry and NanoScience Center Wu, Chao ; National Renewable Energy Laboratory, Biosciences Center Hao, Ji; National Renewable Energy Laboratory, Chemistry & Nanoscience Center Blackburn, Jeffrey; NREL, Svedruzic, Drazenka; National Renewable Energy Laboratory,

Extracellular Electron Transfer Across Bio-Nano Interfaces for CO_2 Electroreduction

Zhaodong Li[#], Wei Xiong[‡], Bertrand J. Tremolet de Villers[†], Chao Wu[‡], Ji Hao[†], Jeffrey L. Blackburn[#*], Drazenka Svedruzic[‡*],

[‡]Biosciences Center, [†]Chemistry and Nanoscience Center, and [#]Materials Physics Center - National Renewable Energy Laboratory, 15013 Cole Boulevard, Golden, Colorado 80401, United States

**Corresponding authors: Drazenka Svedruzic, Jeffrey L. Blackburn*

Abstract

Acetogenic bacteria represent a class of organisms capable of converting reducing equivalents and carbon dioxide into products with carbon-carbon bonds. Materials-based bio-electrochemical approaches are attractive for supplying biological organisms directly with grid-supplied electrons to convert carbon dioxide to value-added chemicals. Carbon nanotube-modified biocathodes have emerged as promising candidates for microbial electrosynthesis with high yields of carbon product formation, but a fundamental understanding of extracellular charge transfer at this electrode-biofilm interface is still lacking. Here, we utilize solid-state interfaces between semiconducting single-walled carbon nanotubes (s-SWCNT) and a model acetogenic bacterium for mechanistic studies of electro-catalytic CO_2 conversion to acetate. Studies of bacteria/s-SWCNT interactions in a transistor-based device suggest direct extracellular electron transfer (EET) at the bio-nano interface. Deuterium isotope labeling experiments confirmed that the availability of electrochemically produced H_2 as a redox mediator does not limit the efficiency of EET and CO_2 electro-reduction for *C. ljungdahlii* biofilms, suggesting the primary reducing equivalents are the electrons delivered across the electrode/bacterium interface or involvement of biological redox mediators. Additional isotope labeling studies demonstrate high Faradaic efficiency for CO_2 electro-reduction at the SWCNT/bacterium interface. These results provide important information about EET across the bacterium/material interface in a model biocathode.

Introduction

Reduction of carbon dioxide (CO_2 RR) has emerged as a possible solution for converting intermittent renewable electrons into more energy-rich organic molecules, and this strategy has the added benefit of mitigating the increased atmospheric concentration of a climate-altering gas. A variety of acetogenic bacteria have evolved to fix CO_2 through the Wood-ljungdahlii pathway[1]. In the past decade, researchers have undertaken efforts to couple these CO_2-fixing bacteria to electrodes and/or semiconductors that enable control over the electron flux to the bacteria, either through photoinduced electron transfer[2-5] or *via* electrolytic injection of energetic electrons across a "biocathode" interface (microbial electrosynthesis, MES)[6,7]. In comparison to chemical catalysts, CO_2 reducing biocathodes can convert CO_2 to *multi-carbon* products at high Faradic and carbon conversion efficiencies, at low overpotentials and at neutral pHs.[8,9] Construction of a highly electroactive biocathode requires: *i)* biocompatible support materials with high conductivity, chemical stability and porous 3D structure, *ii*) high bacteria coverage, in a form of electroactive biofilms and *iii)* high rates and efficiencies of electron transfer between a material and biological component of the system (i.e. extracellular electron transfer, EET).[6,8] As such, various porous 3D materials and surface functionalization, either with biocompatible chemical functionalities or nanomaterials, have been utilized for construction of high activity biocathodes.[8,10-17]

Despite the recent advances in biocathode design and performance, fundamental understanding is still lacking as to how support materials affect growth and electroactivity of biofilms, as well as charge transfer occurring across the bacterium/material interface. Different molecular mechanisms involved in cathodic EET between an electrode and bacteria have often been discussed[18], but less often confirmed and characterized experimentally. Charge transfer between a material and bacteria can occur either directly through conductive proteins or indirectly through soluble redox mediators produced either by bacteria or added externally.[19,20] At more reducing potentials, often applied in MES systems, H_2 produced electrochemically *in situ* can act as an EET mediator/electron donor for the CO_2 bio-reducing activities. An electroactive, acetogenic organism *Clostridium ljungdahlii* (*C. lj.)* is especially interesting to study EET considering that none of the known biological systems typically involved in EET (e.g. pili, cytochromes, quinones, membrane bound or excreted hydrogenases) have been identified in the *C. lj*. genome[19]. Since acetogenic organisms such as *C. lj*. are also electroactive at 0 mV RHE [21,22], the degree to which H_2 may serve as an EET mediator is unclear. While H_2-dependent EET has

been confirmed experimentally in some MES systems,[8,23] the importance of H_2 as a redox mediator is still contested in the literature.[6,18]

Here, we form electrocatalytically active *C. lj.* biofilms on carbon electrodes functionalized with s-SWCNTs. Semiconducting SWCNTs are high aspect ratio, bio-compatible semiconductors that can enable both free-floating solution-phase bio-hybrids[24] or highly electroactive and porous solid-state hybrid electrodes for injection of electrons across the bacterium-nanomaterial interface.[8,10,11] A number of recent studies have explored photo-induced EET in solution-phase bacterial hybrids with inorganic nanocrystals (NC).[2,3,5,17] However, in the solid-state such nanocrystals form close-packed arrays with relatively poor charge conduction and limited porosity, which severely limits the achievable electroactive semiconductor/bacterium interfacial area and practical conversion efficiencies of devices.[25] In contrast, our recent studies have demonstrated that porous solid-state networks of s-SWCNTs have exceptionally high conductivity[26,27] and fast interfacial charge transfer rates.[27,28] We hypothesized that these properties, coupled with nanometer-scale diameters and micron-scale lengths, may facilitate direct EET through intimate interactions with biomolecular complexes on the cell membranes.

With this model system in hand, our study addresses some aspects of the mechanism(s) involved in cathodic EET across the material/bacteria interface, along with the effects that an applied potential and surface nanostructuring have on the CO_2 reducing activities of *C. lj.* biofilms. We find that functionalization of carbon electrodes with SWCNTs increases acetate production by ~180%. Transistor-based measurements suggest direct EET across the SWCNT/bacterium interface. Consistently, deuterium labeling demonstrates that the availability of *electrochemically produced* H_2 or D_2 as a redox mediator does not limit the efficiency of EET and CO_2 electro-reduction. We find that biofilm growth under a reducing potential is important for biofilm electrocatalytic activities and acetate production. These results provide important information about EET across the bacterium/nano-functionalized material interface in a model biocathode.

Results and Discussion

Biofilm Formation

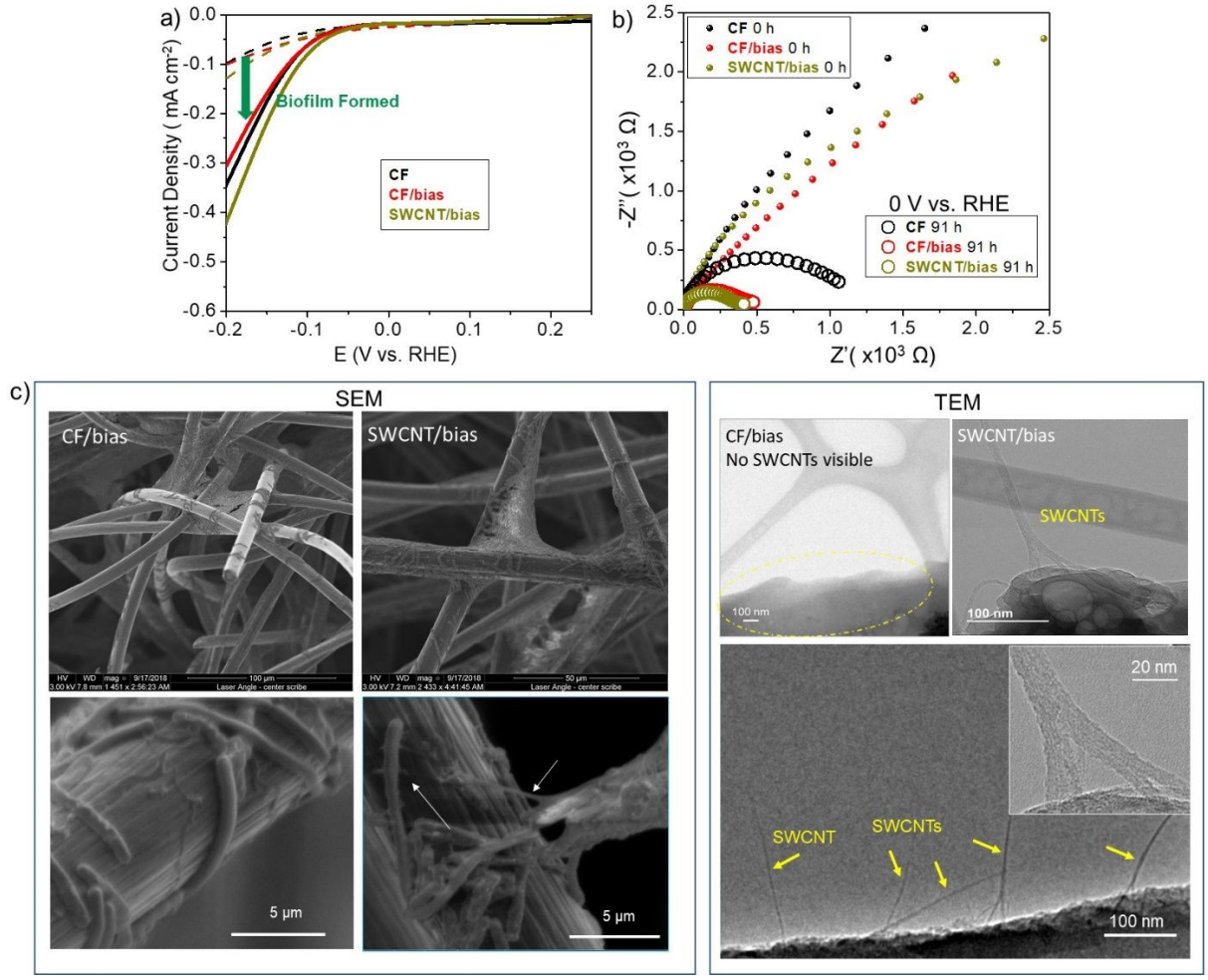

Figure 1. a) Linear sweep voltammetry measurements comparing reducing currents before (dashed lines) and after biofilm growth (solid lines) for CF, CF/bias and SWCNT/bias electrodes, recorded at 5 mVs^{-1}. **b)** Electrochemical impedance spectroscopy (EIS) measurements: Nyquist plots collected at 0h (filled circles) and 91h (open circles) growth for all 3 electrodes. **c)** Representative high-resolution SEM (HRSEM) images at different magnifications for bioelectrode grown on CF and CF/SWCNT electrode matrix showing: dense biofilms growing on and suspended between carbon fibers, individual cells and fibrous structures connecting different bacteria and bacteria to carbon electrodes (CF biocathode showed similar features). **d)** Representative transmission electron microscopy (TEM) images of single bacteria scraped from CF bias and SWCNT/bias electrodes. Zoom on sections of cell membrane with connected SWCNTs bundles. Such bundles were observed only for bacteria grown on SWCNT functionalized carbon felt.

Experiments were conducted either with plain carbon felt (C-felt) or C-felt functionalized with highly enriched semiconducting SWCNTs (C-felt/SWCNT) (see *Methods, Supporting Information, SI*, Fig. S1). SEM images show SWCNT films as hair-like feature, introducing surface nanotopology (Fig S2a,b). We did not detect SWCNT bundles spanning between carbon

fibers. Due to the bacteria size in micrometers, hair-like SWCNT films do not provide additional electroactive surface for bacteria attachment and could theoretically impede it by decreasing contact surface between bacteria and electrode material.[29,30] However, SWCNT films increase overall surface available for CO_2 adsorption[12] and reduction sites for protons and/or any molecular redox mediators involved in EET. Functionalization of CF with SWCNT increases electroactive surface available for small molecules interaction 1.425-fold (Fig S2c).

Biofilms were grown on either C-felt (CF/bias) of C-felt functionalized (SWCNT/bias) (Fig. S3) under a constant reducing potential (-0.7 vs Ag/AgCl). Biofilms were also grown on C-felt without applied potential (CF) in order to test effects of electrical bias on biofilm formation and electrocatalytic activities. Initially, *C. lj.* biofilms were grown from fructose-based media (YTF, see *Methods,* SI) at 37 °C, continuously sparged with a CO_2:N_2 (20:80 mole fraction) gas mixture. Cultures were periodically refreshed to remove planktonic cells and promote continual biofilm formation on the cathode surface[21]. The time-dependent growth of cells in solution and changes in biocathode properties were monitored with optical absorption spectroscopy and electrochemical measurements, respectively (Fig. S4,5). Electrochemical experiments were conducted immediately after media refreshment, to eliminate potential effects from planktonic cells. The linear sweep voltammetry (LSV) data show increase in cathodic currents for all three electrodes with biofilm growth (Fig. 1a), with the most significant reducing currents for SWCNT/bias biocathode. Biofilm growth was also monitored by electrochemical impedance spectroscopy (EIS, Fig. 1b and S6). In the Nyquist plots of Fig. 1b, the diameter of the semicircle at the high-frequency range represents electrochemical polarization resistance of the cathode. Interaction of bacteria with an electrode surfaces displaces the electrolyte layer and changes the physicochemical nature of cathode-electrolyte interface. Even though EIS data for bio-electrodes are difficult to interpret due to contribution of both carbon electrode and biofilm capacitance[31], our data clearly show that biofilm growth dramatically reduces cathodic polarization resistance, consistent with faster reaction kinetics at electrode-electrolyte interface. Notably, biofilms grown on CF with applied bias show significantly smaller polarization resistance than biofilms grown without applied potentials. Sensing of electrode potential and metabolic adaptation by electroactive bacteria have been observed before.[32] Applied bias during growth of *C. lj.* biofilms could induce expression of an electroactive matrix and/or biomolecules involved in

electrochemical reactions on electrode-biofilm interfaces. Additional studies to identify the exact biological mechanism behind this observation are required.[32]

SEM images of biocathodes clearly show rod-shaped *C. lj.* cells, 3-5 μm in length and 0.5-1 μm in width, attached to the electrode matrix (Fig. 1c). Biofilms spanning interstitial space between C-fibers, as well as fibrous biostructures between and directly connecting the cells were visible for all 3 electrodes (CF, CF/bias and SWCNT/bias) and we did not observe specific biofilms' features characteristic for SWCNT-functionalized biocathodes. Bacterium/SWCNT interface was investigated more closely by transmission electron microscopy (TEM). Exclusively for SWCNT biocathodes, ~2-10 nm fibers are attached to the bacteria membranes (Fig. 1c), and the dimensions, fringes and hollow structure of these fibers suggest they are SWCNTs or SWCNT bundles. Based on the TEM images and the fact that SWCNTs were preserved even after the bacteria was scraped off the biocathode, we *speculate* that highly conductive SWCNTs are directly attached to cell membranes. It is not unusual for cells grown in contact with a nanomaterial to integrate nano-structures into bacterial membrane. Previous studies show that SWCNTs can be directly attached or even permeate biological membranes and act as porins to facilitate molecular transport across membranes[33,34].

CO_2 reduction and acetate production by C. lj. biocathodes

Following biocathode fabrication, CO_2 reduction experiments were conducted with all 3 biocathodes (CF, CF/bias, SWCNT/bias) in a minimum media including only inorganic carbon HCO_3^-/CO_2 (*EC phase*, see Supplemental). In these experiments, we track acetate ($C_2H_3O_2^-$) production at an applied potential of -0.05 V vs. RHE with continuous supply of a CO_2:N_2 (20:80) gas mixture. This relatively positive potential (-0.05 V vs RHE) was chosen to minimize H_2 evolution *in-situ* over the carbon surface. Representative LSV results collected after ~100 h in EC phase show that biocathodes with SWCNTs show higher reducing activities and shift in onset potential relative to ones prepared without SWCNT (Fig. 2a). Consistently, total electron consumption (Fig. 2b) and acetate production (Fig. 2c) in >110 h experiments are highest for SWCNT-functionalized electrodes, demonstrating a clear advantage of the SWCNT support for electrolytic CO_2 reduction activity of *C. lj.* biofilms. Average acetate production for SWCNT/bias electrodes was 1.8 fold higher in comparison to CF/bias electrodes (Fig. 2c). Furthermore, biofilms prepared under reducing potential show significantly higher acetate production rates than biofilms

prepared without applied potential. Increases in biocathode activities for SWCNT-functionalized electrodes were demonstrated previously and the effects are typically assigned to an increase in overall electroactive surface available for bacteria attachment,[11,14,16] which does not appear to be the case in our system.

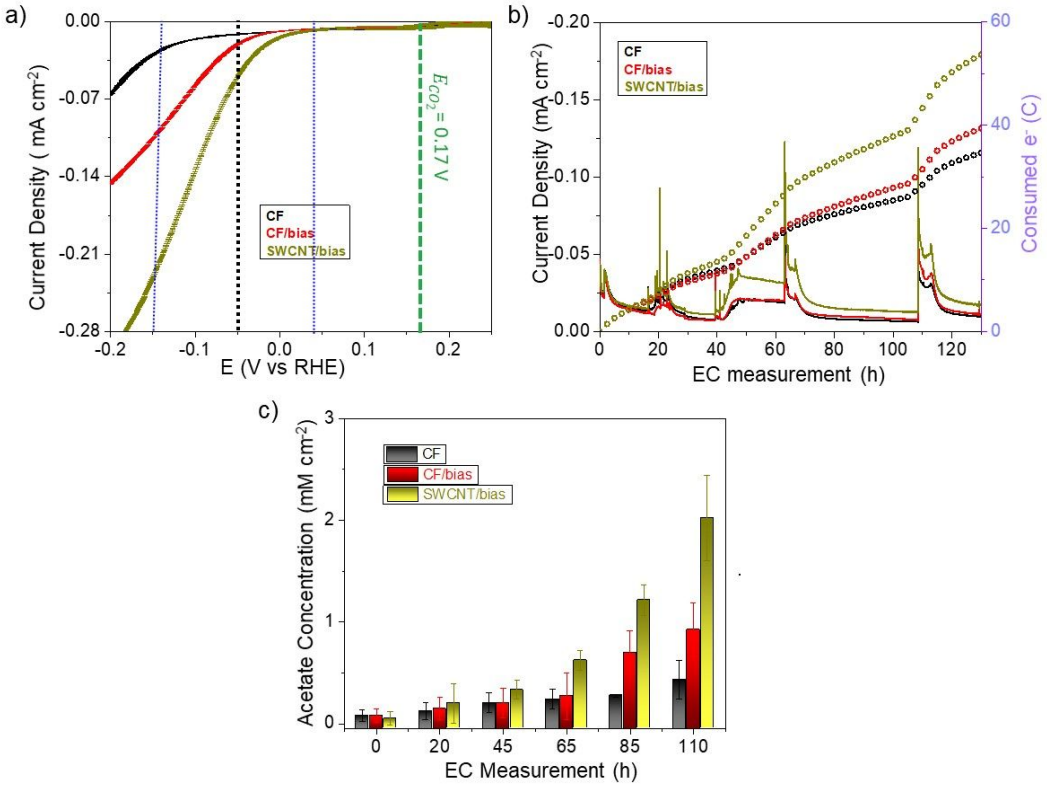

Figure 2. Effects of bias and SWCNTs on microbial electrosynthesis (MSE) process in the EC phase. **a)** Representative LSV data from the EC phase. Collected after 100 h in EC phase. Vertical lines mark the potentials used in this work: black-EC phase, blue-deuterium exchange experiments described later in the text and green-standard CO_2 reducing potential. **b)** Amperometric i-t curves and corresponding overall electrons consumption for 3 different biocathodes under constant reducing potential (-0.05 V vs. RHE). Electron consumption was calculated by integration of i-t curve. Sharp peaks due to charging currents correspond to time points at which the experiment was temporarily stopped/restarted to refresh the media **c)** Time dependent concentration of produced acetate measured in solutions. Averages and errors for 3 separate series of experiments for each electrode are shown.

FET experiments: probing charge transfer across SWCNT/bacteria interface

Encouraged by apparent intimate contact between SWCNTs and *C. lj.* cell membranes (Fig. 1) and improved CO_2 reduction activities for SWCNT-interface *C. lj* biofilms, we set out to probe the degree to which direct EET across the s-SWCNT interface drives the MES process. The semiconducting nature and high charge carrier mobility[35] of our SWCNT scaffolds allow us to fabricate field-effect transistors (FETs) where the carrier type and density can be sensitively tuned

via electrostatic gating. As such, we utilized the approach of making a hybrid electrochemical transistor, as recently demonstrated for probing EET in *Shewanella oneidensis* MR-1 bacteria.[36] These experiments utilized bottom-gated FET devices (Fig. 3a and supporting information), and *C. lj* biofilms were grown directly on the high-mobility s-SWCNT FET channels as discussed above. Figure 3b shows an FET transfer curve of a bacteria-modified s-SWCNT scaffold under 'standard' conditions where the gate voltage modulates source-drain current at a constant source-drain bias. In the ambipolar FET, electrons accumulate and transport within the channel for positive gate voltages, whereas negative potentials foster hole accumulation and transport. In the electrochemical FET configuration, the potential of the SWCNT/bacteria biocathode is modulated in solution by the gold source/drain electrode pair, relative to separate reference and counter electrodes (Ag/AgCl and Pt, respectively), by using typical three-electrode configuration (Fig. 3a, S3b). Figures 3c and 3d show schematics of an electrochemical FET fabricated from a bacteria-modified s-SWCNT channel that is poised at either positive or negative gate biases. It is important to note that the gate bias in these experiments modulates the carrier type and density within the s-SWCNT channel and that *the large gate voltages are not applied directly to the bacteria*.

If direct injection of s-SWCNT carriers into the bacteria is the primary driver of EET and MES, then the catalytic current density and acetate production rate should depend on the carrier type and chemical potential within the s-SWCNT scaffold. As such, we would expect catalytic current densities and CO_2 conversion rates to acetate to be appreciably larger under positive gate biases that lead to electron accumulation in the s-SWCNT network than for negative gate biases that lead to hole accumulation in the s-SWCNTs. The results Figures 3e-g support this hypothesis. Catalytic current density systematically increases as the gate bias is swept from negative to positive (Fig. 3e), which leads to a shift in the onset potential to more positive biases (Fig. 3f). Figure 3g demonstrates that this increased catalytic activity at positive gate potentials translates directly into higher acetate product yields. Figure 3e-g clearly show that the type and density of the charge carriers within the s-SWCNT conducting scaffold dictate the catalytic CO_2 conversion rates within the attached *C. lj* biofilm. These results point towards a mechanism involving direct EET across the s-SWCNT/bacteria interface.

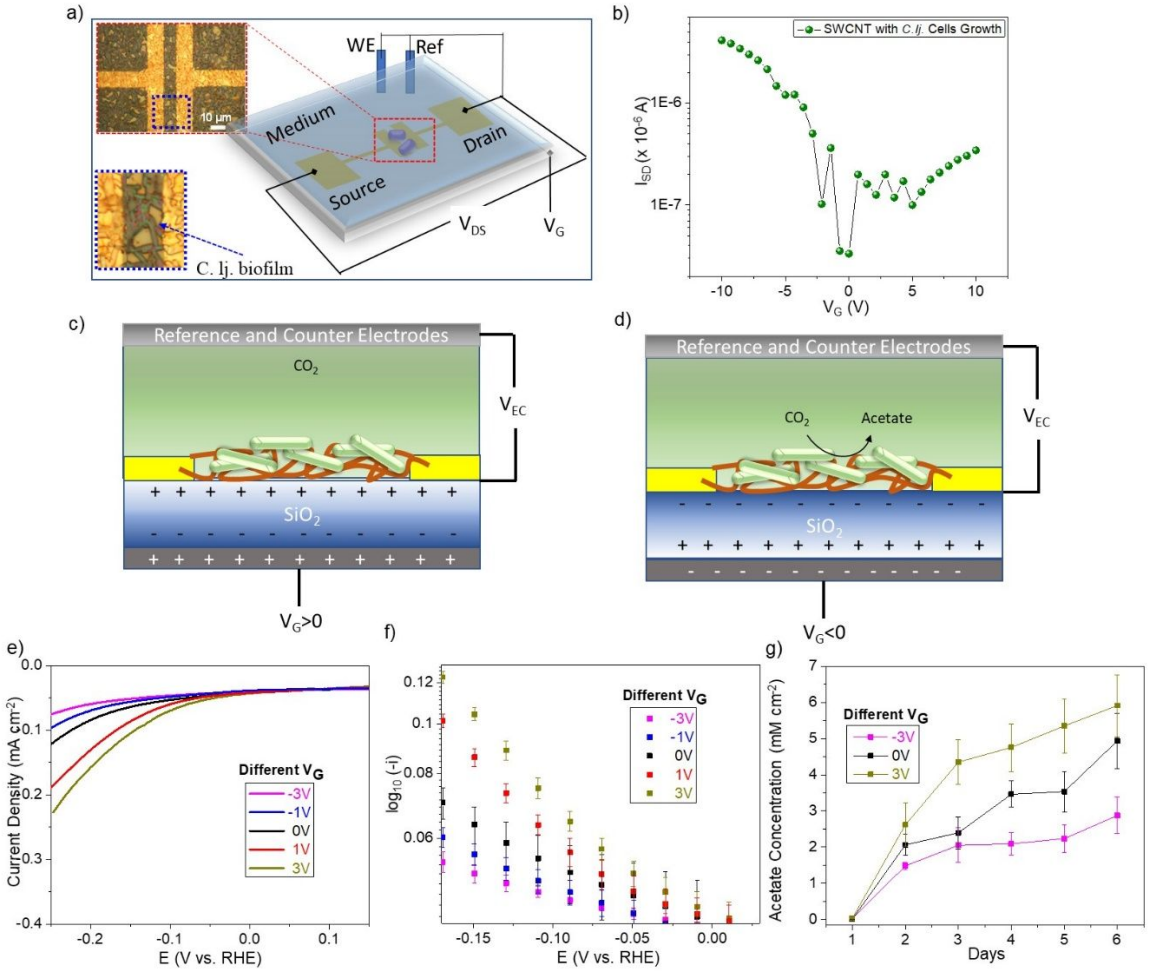

Figure 3. a) Scheme showing the bacteria-modified s-SWCNT FET device for charge transfer interaction investigation (also S3b). The inset photos on the left show microscope images of the 10 μm *C.lj.* modified s-SWCNT channel after growth phase. **b)** FET transfer curve of bacteria-modified s-SWCNT network. **(c)** Schematic of electrochemical FET under positive gate bias. **(d)** Schematic of electrochemical FET under negative gate bias. (e)-(g) Effects of applied V_G on **(e), (f)** linear sweep voltammetry results, **and (g)** acetate production in electrochemical FET experiment. Source/drain potential applied on biofilms was -0.05V vs RHE,

The role of H_2 in EET

Our results discussed thus far suggest that direct EET across the SWCNT/bacteria interface plays an important role in catalytic CO_2 reduction for SWCNT-modified biocathodes. At reducing potentials, H_2 produced electrochemically on the cathode surface can also potentially be utilized by the biofilm as a redox mediator/electron donor for EET.[8] To examine the degree to which electrochemically generated H_2 serves as a redox mediator for *C. lj* biofilms, we turn to deuterium labeling experiments. Specifically, we conducted MES experiments for CF/bias and SWCNT/bias electrodes where the PETC minimum media contained 20% deuterium oxide (D_2O). The potential

was poised at either at -0.15 V or 0.04 V (vs. RHE) and deuterated acetate product was measured with GC-MS (see Methods in SI). D_2 (or HD) is produced electrochemically *in situ* at -0.15 V (vs. RHE), whereas an alternative EET mechanism would be required at 0.04 V where H_2 evolution reaction (HER) is negligible (Fig. 2a, S7a). Using a CF/bias biocathode as an example, Fig 4a shows that the fraction of deuterium-labeled acetate steadily increased during the MES experiment at both potentials, with the most significant increase after 160 h. The *total acetate production* was consistently higher at -0.15 V in comparison to 0.04 V (vs. RHE) (Fig S7b), which can be expected considering a higher thermodynamic driving force at more negative potentials regardless of the mechanism by which reducing equivalents are consumed. Nevertheless, after ~50 h the *fraction of deuterated acetate* produced at -0.15V (vs. RHE) was significantly lower than that produced at 0.04V (vs. RHE) (Fig 4b). Since the amount of D_2/HD produced at -0.15V should be substantially higher than that produced at 0.04V, these results suggest that the availability of H_2 as a redox mediator does not limit the efficiency of EET and CO_2 electro-reduction.

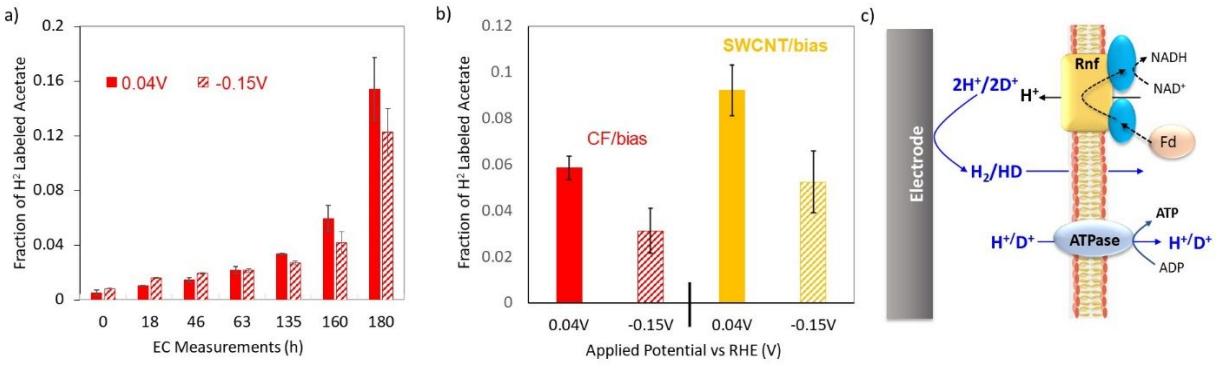

Figure 4. a) ^2H labeled acetate as a fraction of total acetate produced during EC phase for CF/bias electrodes. Error bars were calculated based on two separate series of experiments. **b)** Comparison of ^2H labeled acetate fraction for CF/bias and SWCNT/bias electrode after ~150 h. Error bars were calculated based on 3 and 2 separate series of experiments for 0.04V and -0.15V, respectively. **c)** Scheme showing possible mechanisms by which deuterium can enter cells; Rnf and ATPase are membrane protein complexes involved in proton chemiosmosis, redox balancing and energy production associated with EET.

Naturally, deuterium atoms diffuse into the cell as D^+ or D_2O through chemiosmosis (Scheme in Fig. 4c). CO_2 reduction through WL pathway is coupled to membrane-bound proton pumps Rnf and ATPases involved in energy/redox homeostasis synergistic to electrotrophy and CO_2 reduction. Higher fractions of deuterated acetate at 0.04V for SWCNT/bias biocathodes could be coupled to higher activities of ATPases, which under reducing conditions pumps protons inside the cell. Higher fraction of deuterated acetate for SWCNT/bias biocathodes than CF/bias biocathodes could be due to the higher CO_2 reducing activities or increased diffusion of D_2O/D^+

through cell membranes by SWCNTs acting as a porins.[33] The effects of applied potential and SWCNTs on either of these processes is intriguing and will be explored further. Even though acetate deuteration can be explain by multiple processes, the significantly suppressed deuteration at -0.15V for both biocathodes strongly suggests a non-H_2 mediated EET mechanism for *C. lj*.

^{13}C isotope labeling experiments

From the very beginning of the EC phase we observed high concentrations of ethanol in solution (Fig S9). Due to biocathode preparation in the rich YTF media (i.e. *biofilm growth phase*), it is possible that ethanol accumulates intracellularly and carries over into the *EC phase* despite extensive washing of the biocathodes. The same phenomenon was observed in the literature previously, but was not critically analyzed.[37] We explore contribution of alternative carbon substrates, such as accumulated ethanol and carbon from the scaffold/electrode material, on acetate production *via* ^{13}C isotope labeling experiments. To quantify Faradaic efficiencies for acetate production *directly from* CO_2 ($\delta_{Acetate}$) we conducted experiments with $^{13}CO_2$. In these experiments, the CO_2 sparging gas contained 9.5 % $^{13}CO_2$ and the product included a mixture of ^{12}C and ^{13}C labeled acetate (Fig S10, Table S1). The highest acetate production activities for SWCNT/bias biocathodes resulted in $\delta_{Acetate}$ values of 522 $mMm^{-2}day^{-1}$, which is comparable to other fibrous carbon electrodes with/without SWCNT functionalization, conducted at high potentials -0.05 V *vs.* RHE.[8,21] Faradic efficiencies for CF, CF/bias, and SWCNT/bias electrodes were 52%, 71%, and 91 %, respectively during 20-26 hours in the *EC phase* at constant applied potential -0.05V vs RHE (See SI for details). Experiments with ^{13}C labeled ethanol ($^{13}CH_3{}^{13}CH_2OH$) show ethanol conversion to ^{13}C labeled acetate, which might explain decrease in ethanol concentrations during EC phase (Fig S9). More detailed study of this phenomenon will be given in a separate publication. We also considered the potential role of the carbon-based substrate by synthesizing 100% ^{13}C-labeled SWCNTs in-house. Acetate labeling results (Fig S12) showed that *C. lj.* biofilms do not extract any ^{13}C from the ^{13}C s-SWCNT support.[38]

Discussion: Effects of SWCNT functionalization on CO_2 reducing activities

Our data demonstrate that *C. lj.* biofilm MES activities are improved by (1) the application of a cathodic bias during the growth step and (2) immobilization on semiconducting SWCNT networks. In general, higher MES activities can be attributed to higher biofilm coverages and/or

improved biofilm electrocatalytic activities. To examine which effect is more prominent, we have estimated bacterial coverages for each biocathode based on SEM images, utilizing the method demonstrated before[2,39] and described in the *Supplemental*. The results for biofilm coverages were compared to the acetate production (Table 1). The data show the highest acetate production activities for SWCNT/bias biocathode when normalized for biofilm surface coverage, showing beneficial effects of SWCNT-functionalization other than increasing available surface for bacteria attachment, which is consistent with improved EET in the presence of nanotubes (see earlier discussion of FET data). Acetate production per cell is significantly lower for CF electrodes than for CF/bias electrodes, suggesting that applied potential during biofilm growth has a significant effect on cells ability to reduce CO_2.

Table 1. Comparison of acetate production rate ($\delta_{Acetate}$) and biofilm coverages (σ) for four biocathodes. γ represents average acetate production rates normalized by bacteria coverages Data are collected based on ^{13}C-acetate production from $^{13}CO_2$.

Biocathode	$\delta_{Acetate}$ (mM day^{-1} cm^{-2})	σ (cells μm^{-2})	γ (cell^{-1} s^{-1})
CF	0.0166 ± 0.014	0.1736 ± 0.08	(4.33 ± 0.10) ×10^5
CF/bias	0.0261 ± 0.011	0.1964 ± 0.08	(6.79 ± 0.08) ×10^5
SWCNT/bias	0.0507 ± 0.013	0.1956 ± 0.06	(1.32 ± 0.05) ×10^6

Conclusion

To summarize, we have demonstrated that semiconducting single wall carbon nanotubes serve as a versatile biocompatible scaffold for *C. lj.* biofilm immobilization and electrosynthesis. We find that biofilms grown on SWCNT-modified biocathodes under constant applied negative bias produce the highest CO_2-derived acetate yields due to the highest biofilm electrocatalytic activities. Hybrid electrochemical FET measurements, enabled by the semiconducting nature of our s-SWCNT scaffold, demonstrate that the SWCNTs can enable direct EET across the material/bacteria interface. Since direct EET does not require H_2 as a redox mediator, deuterium isotope labeling experiments demonstrate that the availability of electrochemically produced H_2 does not limit CO_2 electro-reduction to acetate. ^{13}C-labeling experiments demonstrated high Faradaic efficiency (~91%) for CO_2 electro-reduction by SWCNT-functionalized biocathodes at low overpotential (~180 mV) and confirmed that the SWCNT carbon is not utilized as a substrate

for MES. ^{13}C-ethanol labeling experiments showed that ethanol can be utilized by bacteria synergistically with CO_2 electroreduction. Finally, applying a reducing potential during biofilm growth is advantageous for production of MES active biofilms. Looking forward, this model system can be used in a variety of novel mechanistic and device-based MES systems. The biocompatibility and conductivity of semiconducting SWCNTs can be used to engineer direct EET pathways for a host of other bacteria. The excited state of photoexcited small-diameter semiconducting SWCNTs has enough reducing potential to sensitize CO_2 RR *via* electron transfer to catalytic sites, implying such systems may be useful for bio-hybrid based photocatalytic CO_2 RR. Semiconducting SWCNTs also make exceptionally good field-effect transistors, opening up possibilities for SWCNT/bacteria interfaces as (photo)catalytic biohybrid transistors and detectors.

Methods.

Preparation of s-SWCNT films. Plasma-torch (PT) semiconducting single wall carbon nanotubes (s-SWCNTs) powders were purchased from NanoIntegris (Quebec, Canada). Inks containing dispersed SWCNTs were prepared based on a previous report.[40] Carbon felt (AvCrab Felt G100, Fuel Cell Store) as received was cut into pieces with the rectangular shape of 2 ×1 cm. For SWCNT-functionalization CF pieces were soaked for 2 h in the prepared SWCNT ink. These electrodes were analyzed by Raman mapping to confirm and visualize the increasing SWCNT coverage on C-felt when prepared with higher concentrations inks (Fig S3)

Electrochemical measurements. For electro-bioreactor we used typical H-cells with three-electrode configuration (Fig. S3). As a reference electrode we used aqueous Ag/AgCl (saturated) (CH Instruments, Inc). Counter electrode was flat Pt foil with dimension 1x1 cm^{-2}. A Nafion 117 membrane (Sigma-Aldrich) was used to separate the cathodic from anodic compartment. The purging gas (CO_2:N_2 = 20%:80%) for each chamber could be independently controlled with typical flow rate of 5 sccm.

Preparation of *C. ljungdahlii.* *C. ljungdahlii* DSM 13528 (ATCC 55383) was purchased from the *German Collection of Microorganisms and Cell Cultures* (DSMZ) and maintained by freezing mid-log-phase cultures at −80 °C with 10% dimethyl sulfoxide (DMSO) for long-term storage. An

inoculum of *Clostridium ljungdahlii* (10% (v/v) *C. ljungdahlii* DMSO stock) was grown under strict anaerobic conditions in 20 ml modified YTF (**Y**east extract-**T**ryptone-**F**ructose) media (See SI for the detailed composition) in a batch tube at 37 °C.

EC phase. After the *C. ljungdahlii* biocathodes preparation (See SI for details), they were taken out of YTF media and gently washed with phosphate-buffered saline (PBS) solution. Biocathodes were inserted in modified 1754 PETC media (ATCC) and experiments were run at constant reducing potential -0.05 V vs RHE (amperometric i-t measurements). Other conditions were identical to *Growth Phase*. Periodically (every ~24 hours) 1 ml aliquots were taken to measure acetate and ethanol in solution. LSV measurements were also conducted to monitor biofilm electroactivities. During the experiment, the applied potential was interrupted temporarily to collect aliquots and conduct LSV measurements, which caused the spikes in the i-t curves. At each test point, the pH of the electrolyte was monitored.

Field-effect transistor set-up and measurements. The semiconductor single-walled carbon nanotube (SWCNT) field-effect transistor (FET) device was fabricated by using an ultrasonic spray coater to spray as-prepared plasma torch-sSWCNT inks to pre-patterned 200 nm SiO_2/Si substrate. SiO_2/Si substrate is fabricated by using standard microfabrication process in the cleanroom. The electrode is prepared by depositing 5nm Ti/20nm Au through thermal evaporation. There are three channels on each device chip. The dimension of channel tested in this study is 10 μm (width) × 1000 μm (length). The biofilms were grown on s-SWCNT FET as follows: the source, drain and gate contacts were connected with Cu wires. Next, FET device was sealed with epoxy leaving only the s-SWCNT deposited channel area exposed. Biofilms are prepared under the same conditions as described earlier for the growth phase, with source or drain pad connected to the potentiostat working electrode (WE) channel (Fig. S4). The device was immersed in the catholyte contained *C.lj.* culture. Once biofilms were formed, the FET device was gently washed with PBS buffer. The exposed bacteria-modified s-SWCNT channel area was filled with modified PETC medium (as in the EC phase) for the charge transfer test. FET measurements were conducted with a probe station platform, two Keithley 2400 source meters, and a laptop with LabVIEW control programs, and the whole system is built and studied in the nitrogen-filled glovebox. For FET measurements the gate voltage (V_G) is swept in the range -10V to 10V, with sweep rate 4.41V/s.

Thereafter, the device was used as working electrode for EC phase process (see above method details), where the different constant gate voltages (-3V, 0V, -3V) were applied during the whole process. LSV were recorded and samples were collected every day to analyze the production of acetate acid.

Chemical Analysis. Products, acetate and ethanol (*Growth* and *EC Phase*) were analyzed by high-performance liquid chromatography (HPLC, Agilent Technologies). H_2 produced electrochemically, was measured in the headspace by gas chromatography (7890A GC system, Agilent Technologies).

Isotope Experiments. 20% D_2O was added to cathode electrolyte during the EC phase, with biocathodes kept at two different potentials (-0.6 or -0.8 *vs.* Ag/AgCl). D_2O concentrations above 20% were not used due to D_2O toxicity to *C. ljungdahlii* cells. The gas chromatography-mass spectrometry (GC-MS) was utilized to analyze the labeled H in the products.^{13}C-labeled CO_2 (99%, Cambridge Isotope Laboratories) was added (~ 9.5%) to the purging gas during the growth and EC phase to monitor the CO_2 reduction and incorporation into products. ^{13}C-labeled/^{12}C-labeled acetate ratio was measured by gas chromatography-mass spectrometry (GC-MS) and ^{13}CNMR techniques before and after the $^{13}CO_2$ sparging period.

More detailed protocols can be found in the Supplemental section.

Authors contribution

WX, JB and DS conceptualized the project; ZL was involved in all experimental work planning, execution and data analysis; DS helped with electrochemical experiments; TVB conducted Raman analysis; WX, CW conducted MS analysis; JH helped with FET experiments; WX helped with cells culturing and experiments planning; ZL, DS and JB prepared manuscript; DS and JB managed the project.

Acknowledgements

We thank Bennett Addison from NREL for help with analysis of ^{13}C labeled ethanol. This work was authored by the National Renewable Energy Laboratory, operated by Alliance for Sustainable

Energy, LLC, for the U.S. Department of Energy (DOE) under Contract No. DE-AC36-08GO28308. Funding obtained through Laboratory Directed Research and Development program, project number: 0600.10009.18.40.01 (BA and WX were also funded by project 0600.10001.20.77.01). The views expressed in the article do not necessarily represent the views of the DOE or the U.S. Government. The U.S. Government retains and the publisher, by accepting the article for publication, acknowledges that the U.S. Government retains a nonexclusive, paid-up, irrevocable, worldwide license to publish or reproduce the published form of this work, or allow others to do so, for U.S. Government purposes.

Competing interests

The authors declare no competing interests.

Additional information

Supplementary information is available.

Correspondence and requests for materials should be addressed to and Jeffrey L. Blackburn and Drazenka Svedruzic

References

1 Ragsdale, S. W. & Pierce, E. Acetogenesis and the Wood–Ljungdahl pathway of CO2 fixation. *Biochimica et Biophysica Acta (BBA) - Proteins and Proteomics* **1784**, 1873-1898, doi:https://doi.org/10.1016/j.bbapap.2008.08.012 (2008).

2 Liu, C. *et al.* Nanowire–Bacteria Hybrids for Unassisted Solar Carbon Dioxide Fixation to Value-Added Chemicals. *Nano Letters* **15**, 3634-3639, doi:10.1021/acs.nanolett.5b01254 (2015).

3 Kornienko, N. *et al.* Spectroscopic elucidation of energy transfer in hybrid inorganic-biological organisms for solar-to-chemical production. *Proc Natl Acad Sci U S A* **113**, 11750-11755, doi:10.1073/pnas.1610554113 (2016).

4 Zhang, H. *et al.* Bacteria photosensitized by intracellular gold nanoclusters for solar fuel production. *Nature Nanotechnology* **13**, 900-905, doi:10.1038/s41565-018-0267-z (2018).

5 Ding, Y. *et al.* Nanorg Microbial Factories: Light-Driven Renewable Biochemical Synthesis Using Quantum Dot-Bacteria Nanobiohybrids. *Journal of the American Chemical Society* **141**, 10272-10282, doi:10.1021/jacs.9b02549 (2019).

6 Bian, B., Bajracharya, S., Xu, J., Pant, D. & Saikaly, P. E. Microbial electrosynthesis from CO2: Challenges, opportunities and perspectives in the context of circular bioeconomy. *Bioresource Technology* **302**, 122863, doi:https://doi.org/10.1016/j.biortech.2020.122863 (2020).

7 Prévoteau, A., Carvajal-Arroyo, J. M., Ganigué, R. & Rabaey, K. Microbial electrosynthesis from CO2: forever a promise? *Current Opinion in Biotechnology* **62**, 48-57, doi:https://doi.org/10.1016/j.copbio.2019.08.014 (2020).

8 Flexer, V. & Jourdin, L. Purposely Designed Hierarchical Porous Electrodes for High Rate Microbial Electrosynthesis of Acetate from Carbon Dioxide. *Accounts of Chemical Research*, doi:10.1021/acs.accounts.9b00523 (2020).

9 Bajracharya, S. *et al.* Biotransformation of carbon dioxide in bioelectrochemical systems: State of the art and future prospects. *Journal of Power Sources* **356**, 256-273, doi:https://doi.org/10.1016/j.jpowsour.2017.04.024 (2017).

10 Zhang, T. *et al.* Improved cathode materials for microbial electrosynthesis. *Energy Environ. Sci.* **6**, 217-224, doi:10.1039/c2ee23350a (2013).

11 Jourdin, L. *et al.* A novel carbon nanotube modified scaffold as an efficient biocathode material for improved microbial electrosynthesis. *Journal of Materials Chemistry A* **2**, 13093-13102, doi:10.1039/C4TA03101F (2014).

12 Jourdin, L. *et al.* High Acetic Acid Production Rate Obtained by Microbial Electrosynthesis from Carbon Dioxide. *Environmental Science & Technology* **49**, 13566-13574, doi:10.1021/acs.est.5b03821 (2015).

13 Aryal, N., Halder, A., Tremblay, P.-L., Chi, Q. & Zhang, T. Enhanced microbial electrosynthesis with three-dimensional graphene functionalized cathodes fabricated via solvothermal synthesis. *Electrochimica Acta* **217**, 117-122, doi:https://doi.org/10.1016/j.electacta.2016.09.063 (2016).

14 Bian, B. *et al.* Porous nickel hollow fiber cathodes coated with CNTs for efficient microbial electrosynthesis of acetate from CO2 using Sporomusa ovata. *Journal of Materials Chemistry A* **6**, 17201-17211, doi:10.1039/C8TA05322G (2018).

15 Aryal, N., Ammam, F., Patil, S. A. & Pant, D. An overview of cathode materials for microbial electrosynthesis of chemicals from carbon dioxide. *Green Chemistry* **19**, 5748-5760, doi:10.1039/C7GC01801K (2017).

16 Han, S., Liu, H., Zhou, C. & Ying, H.-j. Growth of carbon nanotubes on graphene as 3D biocathode for NAD+/NADH balance model and high-rate production in microbial electrochemical synthesis from CO2. *Journal of Materials Chemistry A* **7**, 1115-1123, doi:10.1039/C8TA10465D (2019).

17 Sahoo, P. C., Pant, D., Kumar, M., Puri, S. K. & Ramakumar, S. S. V. Material–Microbe Interfaces for Solar-Driven CO2 Bioelectrosynthesis. *Trends in Biotechnology* **38**, 1245-1261, doi:https://doi.org/10.1016/j.tibtech.2020.03.008 (2020).

18 May, H. D., Evans, P. J. & LaBelle, E. V. The bioelectrosynthesis of acetate. *Current Opinion in Biotechnology* **42**, 225-233, doi:https://doi.org/10.1016/j.copbio.2016.09.004 (2016).

19 Kracke, F., Vassilev, I. & Krömer, J. O. Microbial electron transport and energy conservation – the foundation for optimizing bioelectrochemical systems. *Frontiers in Microbiology* **6**, doi:10.3389/fmicb.2015.00575 (2015).

20 Tremblay, P.-L., Angenent, L. T. & Zhang, T. Extracellular Electron Uptake: Among Autotrophs and Mediated by Surfaces. *Trends in Biotechnology* **35**, 360-371, doi:https://doi.org/10.1016/j.tibtech.2016.10.004 (2017).

21 Nevin, K. P., Woodard, T. L., Franks, A. E., Summers, Z. M. & Lovley, D. R. Microbial Electrosynthesis: Feeding Microbes Electricity To Convert Carbon Dioxide and Water to

Multicarbon Extracellular Organic Compounds. *mBio* **1**, e00103-00110, doi:10.1128/mBio.00103-10 (2010).
22 Nevin, K. P. *et al.* Electrosynthesis of Organic Compounds from Carbon Dioxide Is Catalyzed by a Diversity of Acetogenic Microorganisms. *Applied and Environmental Microbiology* **77**, 2882-2886, doi:10.1128/aem.02642-10 (2011).
23 Blanchet, E. *et al.* Importance of the hydrogen route in up-scaling electrosynthesis for microbial CO2 reduction. *Energy & Environmental Science* **8**, 3731-3744, doi:10.1039/C5EE03088A (2015).
24 McDonald, T. J. *et al.* Wiring-Up Hydrogenase with Single-Walled Carbon Nanotubes. *Nano Letters* **7**, 3528-3534, doi:10.1021/nl072319o (2007).
25 Wenzel, T., Hartter, D., Bombelli, P., Howe, C. J. & Steiner, U. Porous translucent electrodes enhance current generation from photosynthetic biofilms. *Nat Commun* **9**, 1299, doi:10.1038/s41467-018-03320-x (2018).
26 Norton-Baker, B. *et al.* Polymer-Free Carbon Nanotube Thermoelectrics with Improved Charge Carrier Transport and Power Factor. *ACS Energy Letters* **1**, 1212-1220, doi:10.1021/acsenergylett.6b00417 (2016).
27 Sulas-Kern, D. B., Zhang, H., Li, Z. & Blackburn, J. L. Microsecond charge separation at heterojunctions between transition metal dichalcogenide monolayers and single-walled carbon nanotubes. *Materials Horizons* **6**, 2103-2111, doi:10.1039/C9MH00954J (2019).
28 Blackburn, J. L. Semiconducting Single-Walled Carbon Nanotubes in Solar Energy Harvesting. *ACS Energy Letters* **2**, 1598-1613, doi:10.1021/acsenergylett.7b00228 (2017).
29 Champigneux, P., Delia, M.-L. & Bergel, A. Impact of electrode micro- and nano-scale topography on the formation and performance of microbial electrodes. *Biosensors and Bioelectronics* **118**, 231-246, doi:https://doi.org/10.1016/j.bios.2018.06.059 (2018).
30 Al-Jumaili, A., Alancherry, S., Bazaka, K. & Jacob, M. V. Review on the Antimicrobial Properties of Carbon Nanostructures. *Materials (Basel)* **10**, doi:10.3390/ma10091066 (2017).
31 Heijne, A. t., Liu, D., Sulonen, M., Sleutels, T. & Fabregat-Santiago, F. Quantification of bio-anode capacitance in bioelectrochemical systems using Electrochemical Impedance Spectroscopy. *Journal of Power Sources* **400**, 533-538, doi:https://doi.org/10.1016/j.jpowsour.2018.08.003 (2018).
32 Hirose, A. *et al.* Electrochemically active bacteria sense electrode potentials for regulating catabolic pathways. *Nature Communications* **9**, 1083, doi:10.1038/s41467-018-03416-4 (2018).
33 Tunuguntla, R. H. *et al.* Enhanced water permeability and tunable ion selectivity in subnanometer carbon nanotube porins. *Science* **357**, 792-796, doi:10.1126/science.aan2438 (2017).
34 Higgins, S. G. *et al.* High-Aspect-Ratio Nanostructured Surfaces as Biological Metamaterials. *Advanced Materials* **32**, 1903862, doi:10.1002/adma.201903862 (2020).
35 Brady, G. J. *et al.* Quasi-ballistic carbon nanotube array transistors with current density exceeding Si and GaAs. *Science Advances* **2**, e1601240, doi:10.1126/sciadv.1601240 (2016).
36 Méhes, G. *et al.* Organic Microbial Electrochemical Transistor Monitoring Extracellular Electron Transfer. *Advanced Science* **7**, 2000641, doi:10.1002/advs.202000641 (2020).
37 Bajracharya, S. *et al.* Carbon dioxide reduction by mixed and pure cultures in microbial electrosynthesis using an assembly of graphite felt and stainless steel as a cathode.

Bioresource Technology **195**, 14-24, doi:https://doi.org/10.1016/j.biortech.2015.05.081 (2015).

38 Maksimova, Y. G. Microorganisms and Carbon Nanotubes: Interaction and Applications (Review). *Applied Biochemistry and Microbiology* **55**, 1-12, doi:10.1134/S0003683819010101 (2019).

39 Wang, F., Hwang, Y., Qian, P. Z. G. & Wang, X. A Statistics-Guided Approach to Precise Characterization of Nanowire Morphology. *ACS Nano* **4**, 855-862, doi:10.1021/nn901530e (2010).

40 Sulas-Kern, D. B., Zhang, H., Li, Z. & Blackburn, J. L. Microsecond charge separation at heterojunctions between transition metal dichalcogenide monolayers and single-walled carbon nanotubes. *Materials Horizons*, doi:10.1039/c9mh00954j (2019).